electronics

MDPI

Article

Unidirectional Hybrid Three-Phase Rectifier with Boost Converter and Coupled Inductor

José Teixeira Gonçalves [1,*], Stanimir Valtchev [2], Euclides Luis [3] and Frede Blaabjerg [4]

1 Departamento de Engenharia Elétrica, Faculdade de Engenharia e Tecnologia (FET), Universidade do Namibe, Namibe 274, Angola
2 Departamento de Engenharia Eletrotécnica e de Computadores, CTS/UNINOVA, FCT, FCT Campus Caparica, Universidade NOVA de Lisboa, 2829-516 Monte Caparica, Portugal; ssv@fct.unl.pt
3 Departamento de Engenharias e Tecnologias, ISPTEC—Instituto Superior Politécnico de Tecnologias e Ciências, Luanda 2850, Angola; euclides.luis@isptec.co.ao
4 Department of Energy Technology, University of Aalborg, Pontoppidanstræde 111, 9220 Aalborg Øst, Denmark; fbl@et.aau.dk
* Correspondence: j.goncalves@uninbe.ao

Abstract: The unidirectional hybrid three-phase rectifier (UHTR) with Boost converter consists of two different rectifiers (Rectifier 1 and 2), where Rectifier 2 consists of modules corresponding to the phases. Each rectifier processes different part of the current waveform at the input, so that the sum of the current waveform parts is sinusoidal, or multilevel. Analyzing existing literature, the UHTR with Boost converter and isolation transformer, is proven as a classic solution with high weight, volume and cost. Therefore, in 2019 the UHTR with Boost converter was proposed, without any isolation transformer. To do this, it was necessary to replace the Boost inductor of each Rectifier 2 module with a coupled inductor. However, the proposed UHTR has not described the coupled inductor in details, neither the control circuit and the decoupling of the power circuit with the control circuit were described. Therefore, this main objective this paper is to provide answers to those aspects, and consequently present the UHTR proposal in a more realistic and practical application way, thus favoring the implementation of the prototype. A simulation of the proposed UHTR with coupled inductor was performed in the PSIM version 12.0 software with a power of 20 kW. The results of the proposed UHTR show that there is no current interaction and it works correctly, having a high PF of 99.92% and low total harmonic distortion of 3.96% at full load. In this way, it is proven that it is possible to implement an UHTR with a Boost converter and using coupled inductor.

Keywords: coupling; harmonic distortion; power factor correction

Citation: Gonçalves, J.T.; Valtchev, S.; Luis, E.; Blaabjerg, F. Unidirectional Hybrid Three-Phase Rectifier with Boost Converter and Coupled Inductor. *Electronics* **2024**, *13*, 1864. https://doi.org/10.3390/electronics13101864

Academic Editors: Jožef Ritonja, Le Zheng and Mohammed Agamy

Received: 16 April 2024
Revised: 6 May 2024
Accepted: 8 May 2024
Published: 10 May 2024

1. Introduction

There are several types of three-phase rectifiers with low harmonic content for use in different types of loads, and they can be classified into two large groups, line-commutated and self-commutated (electronically regulated), as shown in Figure 1 [1,2]. In the case of three-phase line-switched rectifiers, diodes are used as a switching device, being driven by the frequency of the input AC voltage. Self-commutated rectifiers use adjustable switching devices (Thyristor, IGBT, MOSFET) activated through a control system [3]. These rectifiers have good performance such as low THD and high PF, and can meet international standards. They have a problem of complexity (due to the control system) and economic viability when applied to high powers [3]. Some power factor correction techniques have been developed to reduce the harmonic content of some three-phase rectifiers. Figure 1 shows the classification of three-phase rectifiers with reduced harmonic content [1,2]. These three-phase rectifiers can present improvements in THD and PF, and some rectifiers can meet the recommendations of established international standards, as is the case with hybrid three-phase rectifiers (HTR), which is the study objective of this work.

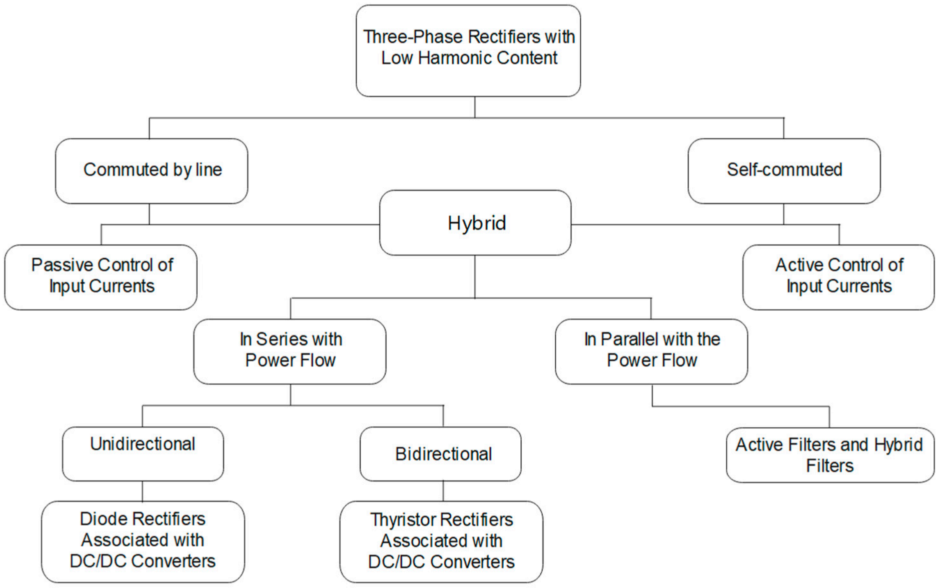

Figure 1. Classification of three-phase rectifiers with low THD [1,2].

HTR can be classified into two large groups, with HTR in series with the power flow and HTR in parallel with the power flow [1], as shown in Figure 1. In the case of this work, it refers to HTR in series with the power flow and it can be classified as unidirectional hybrid three-phase rectifier (UHTR) and bidirectional hybrid three-phase rectifier (BHTR) [1].

The HTR studied understood as rectifiers consisting of two (Rectifier 1 and Rectifier 2) or more rectifiers connected in parallel. In the case of Rectifier 1, it may just be a line-switched bridge rectifier and in other cases it is connected in series with a DC converter to control the output voltage. Rectifier 1 must also be designed so that it processes the largest possible portion of the total energy delivered to the load. Rectifier 2 can be self-commutated (controlling the output voltage) or line-commutated, but connected in series with a DC converter, to control the output voltage, in order to perform active power factor correction and process the remainder of the total energy required by the load. On the other hand, rectifiers must process different current waveforms, so that the sum of the current waveforms reaches the desired one shape (sinusoidal or multilevel) [3–5].

The HTR classification depends on the type of converter applied to Rectifier 2. Therefore, it is possible to obtain an HTR using a Boost, SEPIC, Vienna, Delta-switch, Start-switch and PWM Boost converter on Rectifier 2.

HTR with Boost Converter

UHTR with Boost converter was first proposed in 2005 [4]. It consists of Rectifier 1 associated in parallel with Rectifier 2. Rectifier 1 is a Graetz bridge rectifier with inductive and capacitive filter on the DC bus. The output voltage is not controlled, and it is not possible to impose the shape of the current wave. In this case the value of the output voltage depends on the value of the input voltage and the applied load, the current waveforms depend on the value applied to the inductive filter, in the case of applying a considerably high value to the input current of each phase it can assume a rectangular shape (considering only a half cycle) also due to the conduction of the diodes, which will conduct the electric current in a range of 30° and 150° [6–9]. In the case of Rectifier 2, it consists of three single-phase modules, each module consisting of an isolation transformer, followed by a single-phase rectifier connected in series with a Boost converter having PFC. The isolation transformer at the input of each module (phase) is intended to mitigate current interactions between the converters [6–8,10,11].

The UHTR with Boost converter can impose sinusoidal input currents [7] as well as impose six-level input currents [6,8]. Another alternative to the HTR with Boost converter is to replace the three single-phase transformers with a three-phase transformer, the topology being proposed in [6,8]. The three-phase transformer is low frequency (mains frequency) with the primary windings connected in delta. The authors [6,8] also report the possibility of reducing THD, as with the primary windings connected in delta, it is possible to eliminate the third harmonic current. The study would be interesting, but the authors do not present a detailed study with a prototype, they only presented the structure of the proposed circuit.

Analyzing the HTR with Boost converter and isolation transformer, existing in the literature, it is proven that this classic solution has large weight, volume and also high cost. Therefore, in 2019 [3,4] the HTR was proposed with a Boost converter, but without an isolation transformer. To achieve this, a change was necessary to avoid current interactions between the three modular rectifiers that make up Rectifier 2. The change consists of replacing the Boost converter inductor with a coupled inductor, also implementing a diode in the inverse of the current interaction, thus forcing the current to travel in the normal direction [3,4].

According to the HTR proposal with a Boost converter without isolation transformer, the authors in [3] only limited themselves to present the innovation of mitigating current interactions through the addition of coupled inductor. But it is important to highlight that many important aspects or details have not been developed or validated, described below:

- The coupled inductor was not characterized in details;
- The control circuit applied was not through a specific integrated circuit;
- It was not presented how to eliminate the coupling that may arise between the power circuit and the control circuit.

Therefore, this article's main objective is to provide answers to the aspects presented and consequently present the HTR proposal in a more realistic way, thus favoring the implementation of the prototype.

2. Modeling and Implementation of the Proposed UHTR

The UHTR with Boost converter proposed in this work is composed of three circuits: the power circuit, the interface circuit and the control circuit, which are described below.

2.1. Power Circuit

The purpose of the power circuit is to convert and transfer electrical energy from the AC source to the DC load. The HTR consists of two rectifiers associated in parallel, Rectifier 1 and Rectifier 2, as shown in Figure 2.

Rectifier 1 consists of a Graetz bridge associated with a Boost converter, which allows controlling the output voltage (imposing a stable value) and changes the shape of the current wave at the input to rectangular, as shown in Figure 3a. Rectifier 2 consists of three single-phase rectifiers, each associated with a Boost converter with PFC, and output voltage control, imposing a current waveform at the input, shown in Figure 3b, when added to the shape of the rectangular wave from Rectifier 1 (since they are in parallel), gives rise to a sinusoidal current waveform, as shown in Figure 3c. The control circuit controls Rectifier 1 and Rectifier 2 at the same time by means of the switching switches contained in the Boost converters and the voltage input signals, current input signals, as well as the rectifier output voltage signal. To this end, the connection terminals of the power circuit (see Figure 2) are used with the interface circuit designated as:

- G_{ab} (IGBT gate to connect to Rectifier 1 control circuit);
- G_{a1}, G_{a2}, G_{a3} (IGBT gate to connect to the respective modules of the Rectifier 2 control circuit);
- I_{Lb} (current sensor signal in Rectifier 1 boost converter);
- I_a, I_b, I_C (hybrid rectifier input current sensors signal);
- V_a, V_b, V_c (hybrid rectifier input voltage);
- V_{0+}, V_{0-} (hybrid rectifier output voltage).

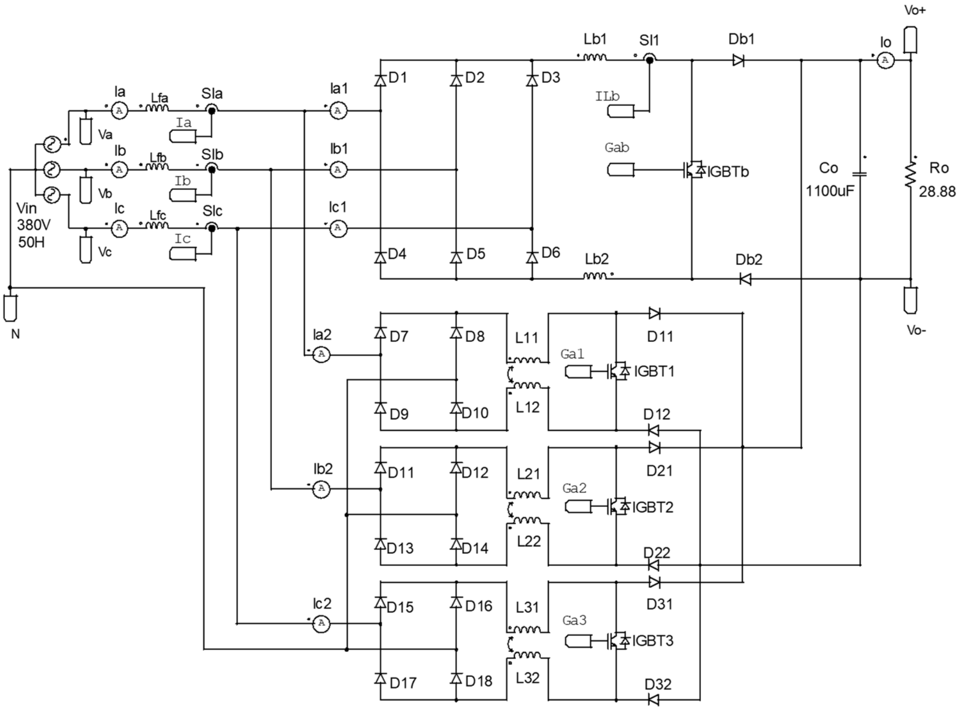

Figure 2. HTR power circuit running on PSIM.

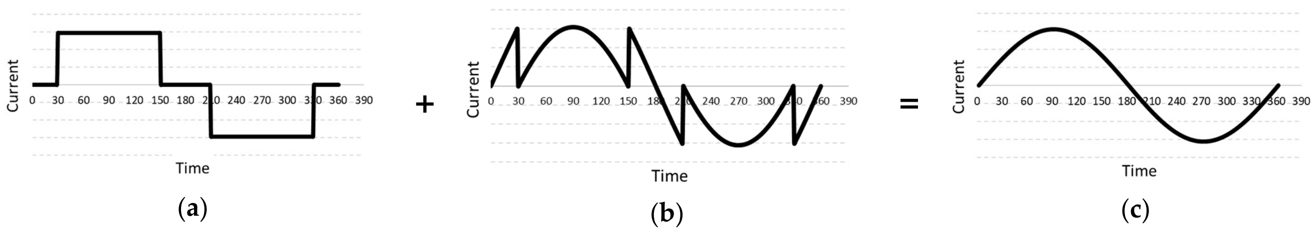

Figure 3. Current waveforms in phase A of the HTR: (**a**) Input current in Rectifier 1; (**b**) Input current in Rectifier 2; (**c**) Input current (sinusoidal) in the HTR.

As previously highlighted, the coupled inductor is the main element of the proposed circuit, as it allows the mitigation of current interaction between Rectifier 2 converters, therefore, the coupled inductor will be detailed more below.

2.1.1. Inductor

The boost inductor L_b of Rectifier 1 is given by [2,12]:

$$L_b = \frac{V_p}{2\ f_s\ \Delta I_{Lb,_{max\%}}\ I_{o1}} \tag{1}$$

where V_p is the peak value of the voltage at the rectifier input; f_s is the switching frequency; $\Delta I_{Lb,_{max\%}}$ is the maximum current variation in the boost inductor; I_{o1} is the output current in Rectifier 1 where, through power distribution between Rectifiers 1 and 2, it is given by:

$$I_{o1} = I_o\ 0.551 \tag{2}$$

Since the Boost converter inductor L_b is divided by two inductors, one for each pole, the inductance of each Boost converter inductor is given by:

$$L_{b1} = L_{b2} = \frac{V_p}{4\ f_s\ \Delta I_{Lb,_{max\%}}\ I_{o1}} \tag{3}$$

In the case of the inductance value of the Boost converter of Rectifier 2, it is given by [2,12]:

$$L_1 = \frac{\overline{\Delta I_{L1}}\, V_{p,min}}{\Delta I_{L1}\, f_S} \tag{4}$$

where $V_{p,min}$ is the minimum peak value of the voltage at the rectifier input; f_s is the switching frequency; ΔI_{L1} is the variation of the Rectifier 2 inductor current; $\overline{\Delta I_{L1}}$ is the normalized current variation of the inductor of module 1 in Rectifier 1, it is given by:

$$\overline{\Delta I_{L1}} = Sin\,\frac{\pi}{2} - \frac{V_{p,min}}{V_o}\, sin^2\,\frac{\pi}{2} \tag{5}$$

Considering that (4) determines the inductance value of the conventional Boost converter, and as the proposed Boost converter is made up of the coupled inductor in a discordant direction, it is important to carry out the study of the coupled inductor in order to determine its inductance.

2.1.2. Discordant Sense Coupled Inductor

Figure 4 illustrates an equivalent scheme of the coupled inductor in a discordant direction, consisting of two inductors (L_{11} and L_{12}) coupled by a toroidal core. The current that runs through the primary inductor L_{11} is the same current (in the opposite direction) that runs through the secondary inductor L_{12}. The flows generated by the inductors and consecutively the mutual flows are also presented. The windings of the inductor wires are discordant in direction and, therefore, much of the mutual flux cancels each other out because they run in opposite directions. The directions of the magnetic fluxes were determined using the right-hand rule. The methodology applied to study the coupled inductors (L_{11} and L_{12}) is based on [12–16].

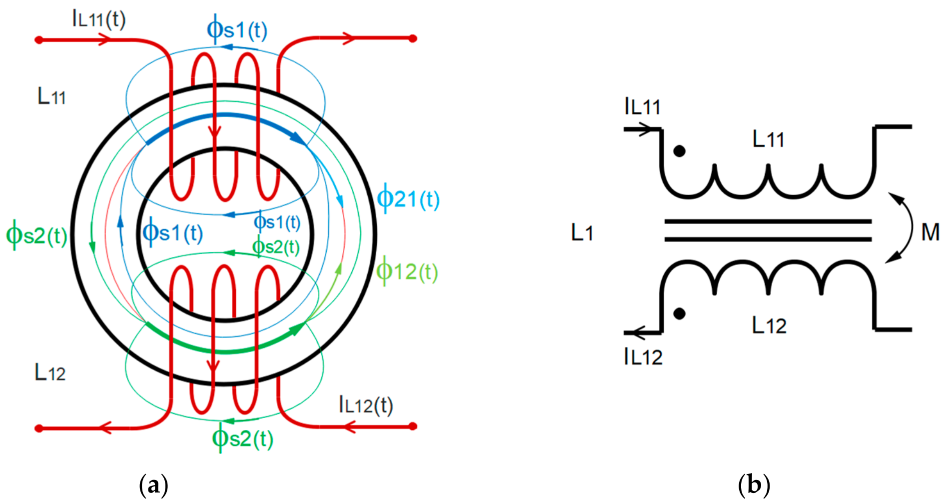

Figure 4. Coupled inductor for Rectifier 2 boost converter module: (**a**) ideal representation of the coupled inductor; (**b**) equivalent representation of the coupled inductor. Where $\phi_{s1}(t)$ is the dispersion flux due to current I_{L11}; $\phi_{21}(t)$ is the flux that covers the inductor L_{12} due to the current I_{L11}; $\phi_{s2}(t)$ is the dispersion flux due to current I_{L12}; $\phi_{12}(t)$ is the flux that covers the inductor L_{11} due to the current I_{L12}.

First, the fluxes are analyzed separately, in the primary inductor and then in the secondary inductor. Thus, analyzing Figure 4a, considering that only the current passes through the primary inductor or secondary inductor, the total flux ($\phi_{11}(t)$) ($\phi_{22}(t)$) are given by:

$$\begin{aligned}\phi_{11}(t) &= \phi_{s1}(t) + \phi_{21}(t) \\ \phi_{22}(t) &= \phi_{s2}(t) + \phi_{12}(t)\end{aligned} \tag{6}$$

Considering the magnetic coupling of the inductors. The total flux in the primary inductor $\phi_1(t)$ and secondary inductor $\phi_2(t)$ are given by:

$$\phi_1(t) = \phi_{11}(t) - \phi_{12}(t) \tag{7}$$

$$\phi_2(t) = \phi_{22}(t) - \phi_{21}(t) \tag{8}$$

The mutual flow between the two inductors, due to the action of current I_{L11} and current I_{L12} on the magnetic coupling. As the flow direction $\phi_{21}(t)$ is opposite to the flow direction $\phi_{12}(t)$, they cancel each other out, thus the mutual flow $\phi_m(t)$ is given by:

$$\phi_m(t) = \phi_{21}(t) - \phi_{12}(t) \tag{9}$$

Replacing (9) in (7) and (8), the value of the total flow $\phi_1(t)$e$\phi_2(t)$, when using the mutual flow $\phi_m(t)$, are given by:

$$\begin{aligned}\phi_1(t) &= \phi_{s1}(t) + \phi_m(t) \\ \phi_2(t) &= \phi_{s2}(t) + \phi_m(t)\end{aligned} \tag{10}$$

The relationship between the fluxes through all the turns of the inductor and the current that passes through the inductors is studied considering the current I_{L11} applied to the primary inductor and then the current I_{L12} applied to the secondary inductor. In the case of applying only the current I_{L11}, where the amount of total flux in the turns of the primary inductor $N_{esp,L11}$ is proportional to the current that passes through the primary inductor, the relationship is given by:

$$N_{esp,L11}\ \phi_{11}(t) = \pm L_{11}\ I_{L11}(t) \tag{11}$$

Considering that the flux ϕ_{21} also passes through the secondary inductor, then the amount of flux ϕ_{21} in the turns of the secondary inductor $N_{esp,L12}$ is directly proportional to the current that passes through the primary inductor and to the mutual induction coefficient in the secondary inductor M_{21} due to current I_{L11}, given by:

$$N_{esp,L12}\ \phi_{21}(t) = \pm M_{21}\ I_{L11}(t) \tag{12}$$

Considering the specific case of the flow only passing through the current I_{L12} in the secondary inductor, it is given by:

$$\begin{aligned}N_{esp,L12}\ \phi_{22}(t) &= \pm L_{12}\ I_{L12}(t) \\ N_{esp,L11}\ \phi_{12}(t) &= \pm M_{12}\ I_{L12}(t)\end{aligned} \tag{13}$$

Multiplying (7) and (8), the total flux of the inductor by the number of turns corresponding to each inductor (13) and deriving as a function of time, given by:

$$\begin{aligned}N_{esp,L11}\ \frac{d\phi_1(t)}{dt} &= N_{esp,L11}\ \frac{d\phi_{11}(t)}{dt} - N_{esp,L11}\ \frac{d\phi_{12}(t)}{dt} \\ N_{esp,L12}\ \frac{d\phi_2(t)}{dt} &= N_{esp,L12}\ \frac{d\phi_{22}(t)}{dt} - N_{esp,L12}\ \frac{d\phi_{21}(t)}{dt}\end{aligned} \tag{14}$$

Applying Faraday's law, the relationship between flows and electrical current intensity is given by:

$$\begin{cases} u_1(t) = N_{esp,L11}\,\frac{d\phi_{11}(t)}{dt} - N_{esp,L11}\,\frac{d\phi_{12}(t)}{dt} = L_{11}\,\frac{dI_{L11}(t)}{dt} - M_{12}\,\frac{dI_{L12}(t)}{dt} \\ u_2(t) = N_{esp,L12}\,\frac{d\phi_{22}(t)}{dt} - N_{esp,L12}\,\frac{d\phi_{21}(t)}{dt} = L_{12}\,\frac{dI_{L12}(t)}{dt} - M_{21}\,\frac{dI_{L11}(t)}{dt} \end{cases} \quad (15)$$

where u_1 and u_2 represent the voltages in the primary and secondary inductor consecutively; M_{12} and M_{21} are the mutual inductances.

Considering that the mutual inductance passing through the primary inductor and secondary inductor is the same, then it is represented by $M = M_{12} = M_{21}$. Thus (15) is given by:

$$\begin{cases} u_1(t) = L_{11}\,\frac{dI_{L11}(t)}{dt} - M\,\frac{dI_{L12}(t)}{dt} = (L_{11} - M)\,\frac{dI_{L12}(t)}{dt} \\ u_2(t) = L_{12}\,\frac{dI_{L12}(t)}{dt} - M\,\frac{dI_{L11}(t)}{dt} = (L_{12} - M)\,\frac{dI_{L11}(t)}{dt} \end{cases} \quad (16)$$

Solving for (16), it is given by:

$$u_T(t) = u_1(t) + u_2(t) = (L_{11} + L_{12} - 2M)\,\frac{dI_{L1}(t)}{dt} \quad (17)$$

The value of the equivalent inductance of the inductor coupled with a discordant direction, given by:

$$L_1 = L_{11} + L_{12} - 2M \quad (18)$$

Knowing that the mutual inductance is given by:

$$M = K\,\sqrt{L_{11}\,L_{12}} \quad (19)$$

The value of the inductances L_{11} and L_{12} of the coupled inductor and the mutual inductance are determined by substituting (19) into (18), given by

$$L_1 = L_{11} + L_{12} - 2\,K\,\sqrt{L_{11}\,L_{12}} \quad (20)$$

Considering that L_{11} and L_{12} have the same modular value ($L_{11} = L_{12}$), then it is represented by L_{11}. Thus, solving (20) the inductance is given by:

$$L_1 = 2\,L_{11} - 2\,K\,L_{11} \quad (21)$$

Factoring (21) the equivalent inductance is given by:

$$L_1 = L_{11}\,(2 - 2\,K) \quad (22)$$

Thus, the primary and secondary inductances are given by:

$$L_{11} = L_{12} = \frac{L_1}{(2 - 2\,K)} \quad (23)$$

Replacing the equivalent inductance L_1 (4) in (23), the primary and secondary inductances ($L_{11} = L_{12}$), which the coupled inductor needs for the proposed type of Boost converter, is given by:

$$L_{11} = L_{12} = \frac{V_{p,min}\,\overline{\Delta I_{L1}}}{f_s\,\Delta I_{L1}\,(2 - 2\,K)} \quad (24)$$

2.2. Interface Circuit

The interface circuit makes it possible to make an isolated connection between the power circuit and the control circuit, so that there are no interactions between the two. To achieve this, it was necessary to implement several electrical circuits and sensors. Therefore, the interface circuit consists of:

- Current sensors: The inductor current signal is obtained by means of current sensors with galvanic isolation. In Rectifier 1, the current sensor is installed on the positive polarity of the Boost converter and, therefore, does not require a precision rectifier, just a polarity inverter, as described in the control circuit. For Rectifier 2, the AC at the input of each phase of the hybrid rectifier is monitored.

- Current precision rectifier: The output signal of the current sensor (AC) is thus rectified by a current precision rectifier (CPR) in negative polarity. The CPR consists mainly of three operational amplifiers, the first two of which are designed for proper rectification and the last is a Buffer circuit [2,17]. Figure 5a shows the CPR of just one phase.
- Voltage precision rectifier: The rms voltages obtained from the voltage sensor were rectified by a precision rectifier in positive polarity. In this case, the precision rectifier mainly consists of three operational amplifiers, the first two of which are designed to rectify the appropriate voltage, and the last one is a Voltage Buffer (voltage follower), as shown in Figure 5b [2,17].
- AC voltage sensor: The input voltage sensors used are transformers in each phase, with a ratio of 220 V/6 V (sensor gain G_V = 0.0273) in star-star configuration, as shown in Figure 6a. In this way, the voltages $V_{a,gv,ef}$, $V_{b,gv,ef}$, $V_{C,gv,ef}$, are obtained, which are images of the input voltages. Three resistors connected in a star are also applied as a load to the output of the transformers, with the central point connected to the ground of the control circuit, serving as a virtual neutral. To avoid high frequency noise above hundreds of Hz, 56 nF capacitors were added in parallel with the resistors.
- DC voltage sensor: To control the output voltage V_o of the DC bus, the output voltage loop circuit is created, which mainly consists of an output voltage sensor (sensor gain, G_{Vo} = 0.00329), a voltage signal amplifier and then the respective voltage compensator $C_V(s)$ [2,17], as shown in Figure 6b.
  According to the methodology for adjusting the C_V voltage compensator parameters, the frequencies determined are:
  - $f_{CV} = 10$ Hz;
  - $f_{ZV} = 2.5$ Hz;
  - $f_{P1V} = 0$ Hz;
  - $f_{P2V} = 300$ Hz.

  Depending on the frequencies, the components of the voltage compensator $C_V(s)$ are determined, shown in Figure 6b.
- Current level regulator circuit: The voltage compensator output voltage V_{CV} can be used to control the current level that the power circuit processes through an additional circuit [4], as is the case with the current level regulator current shown in Figure 7. In this case, the current level regulator allows to regulate (control) the V_{CV} voltage and thus change the current level at the rectifier input. It consists of two circuits, an amplifier and then an inverter, as shown in Figure 7 [2,17]. Although the voltage sensor and voltage compensator are exclusive to the two rectifiers (Rectifier 1 and Rectifier 2), the current level regulator circuit must be one for each rectifier. Thus, as the current level in Regulator 1 changes, the current in Rectifier 2 is compensated, and vice versa [4].
- Feed-forward voltage circuit: The circuit applied to the feed-forward voltage loop is shown in Figure 8a. It can be seen that the circuit consists of a three-resistance voltage adder (to generate the voltage $V_{in,soma,min}$), an operational amplifier (to generate the voltage V_{ffC}) and a voltage divider with a filter (to generate the voltage V_{ff}).
- Programmable reference voltage of Rectifier 1: For Rectifier 1 to impose a current waveform as represented in Figure 3a, it is necessary that the programmable reference voltage injected into the control circuit is a constant voltage and proportional to the voltage effective input, for which the voltage V_{ffc} is used from the feed-forward voltage circuit. The circuit used to generate the programmable reference voltage is represented in Figure 8b.
- On/off control mode circuit.
- Auxiliary sources.

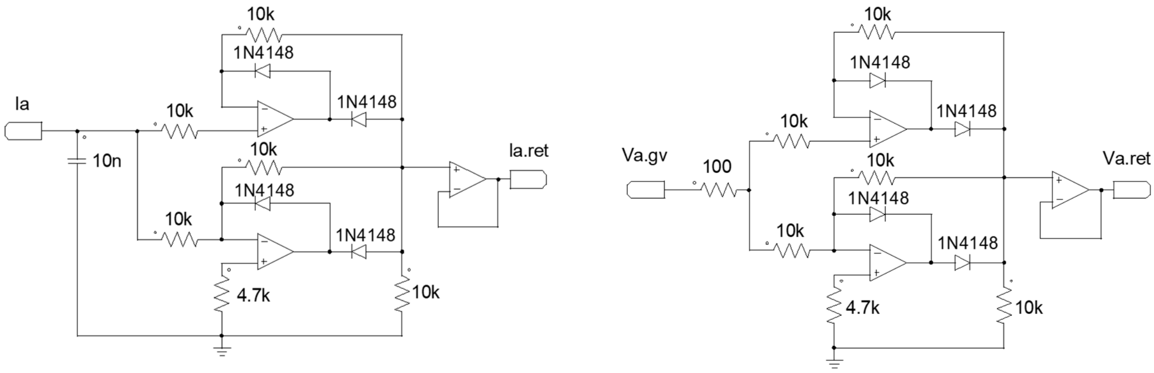

(**a**) (**b**)

Figure 5. Precision rectifier circuit: (**a**) Current precision rectifier in phase A; (**b**) Voltage precision rectifier in phase A.

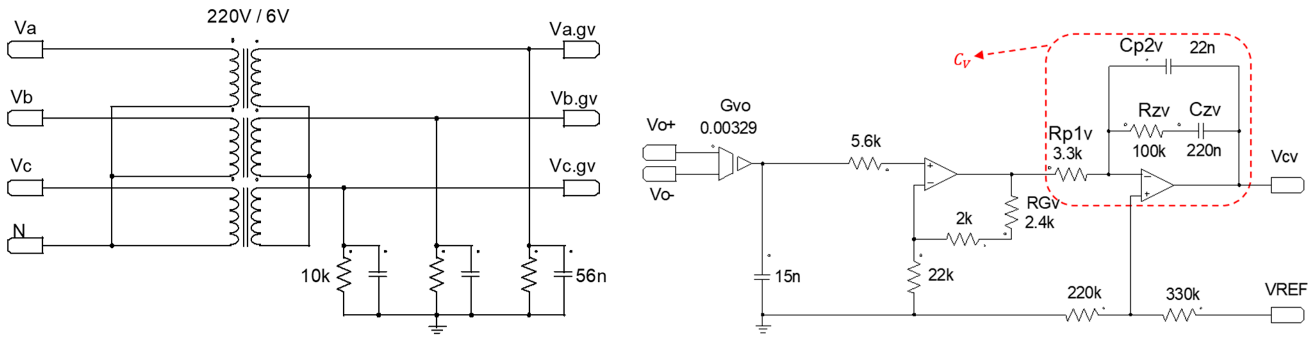

(**a**) (**b**)

Figure 6. Sensor circuit: (**a**) AC voltage sensor; (**b**) DC voltage sensor.

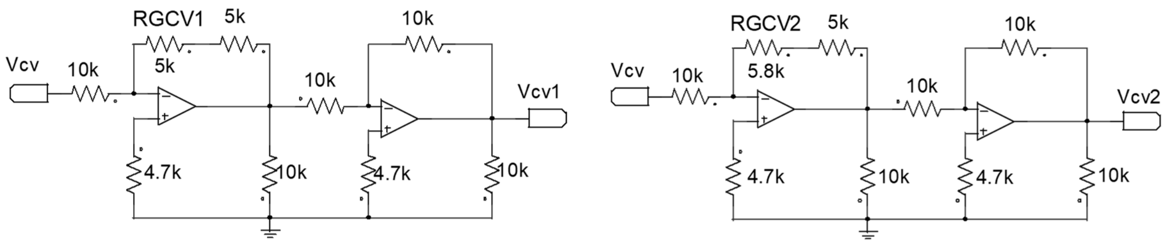

(**a**) (**b**)

Figure 7. Current level regulator circuit: (**a**) Rectifier 1; (**b**) Rectifier 2.

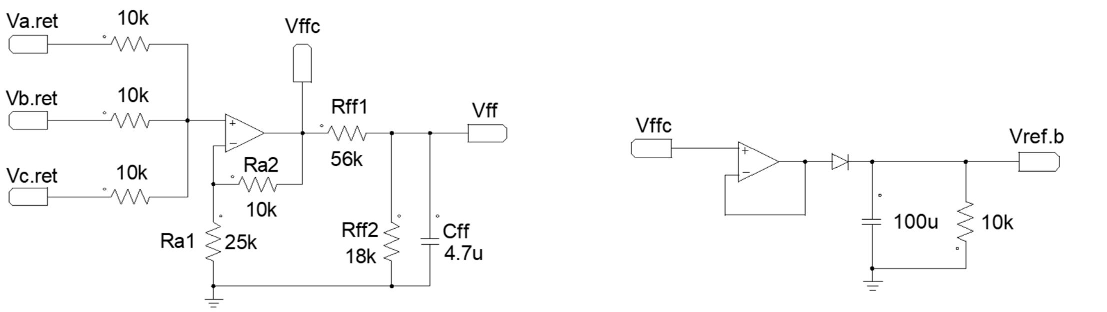

(**a**) (**b**)

Figure 8. Voltage generator circuit: (**a**) Feed-forward; (**b**) Programmable reference for Rectifier 1 control.

2.3. Control Circuit

In the proposed HTR with Boost converter, average current control in continuous conduction mode (CCM) is applied.

The average current control is divided into two loops, a current loop and a voltage loop, in order to generate the PWM signal for the changeover switch (S). The current loop works with two input signals, the inductor current signal being the rectified AC input voltage signal. The voltage loop works with the DC voltage signal from the output and a reference voltage to produce the voltage error signal (ev) required for the current loop.

In the average current control, the inductor current is monitored and filtered by the current compensator (current regulator), which is compared with the reference current signal. Subsequently, the output of the current regulator is compared with the sawtooth signal in the PWM modulator, thus generating the PWM signals for the MOSFET. In this way, the current loop tends to minimize the error between the average value of the input current and its reference current. Note that the reference current is obtained by multiplying the rectified input AC voltage signal by the voltage error (e_V) (obtained from the voltage loop). In this way, a reference signal is obtained that will define the synchronization with the electrical network, the wave shape and its amplitude, in order to obtain a high PF, low THD and output voltage control [18–22].

For the sinusoidal waveform, it is necessary for each HRT rectifier to impose a different waveform, so that when adding the two waveforms, a sinusoidal current shape is obtained. For these forms of currents to be imposed, an appropriate control strategy is necessary. Control systems require current and voltage input signals for both Rectifier 1 and Rectifier 2. Signal distributions are made in the current loop and voltage loop, of Rectifier 1 and Rectifier 2 [23–25]. Distributed as follows:

- For the Rectifier 1 current loop, the Boost 1 inductor current signal (I_{Lb}) is applied;
- For the current loop of Rectifier 2, the input current signals, I_a, I_b, I_c and the reference voltage signals, V_a, V_b, V_c, are applied;
- On the other hand, the V_o signal is applied to the voltage loop to obtain e_V and this is used for the current loop of the two rectifiers.

The important thing in the control strategy is to make the current control of Rectifier 2 follow the same waveform as the sinusoidal input voltage, through the signals I_a, I_b, I_c and the reference voltage signals, V_a, V_b, V_c. Therefore, Rectifier 2 current is a sinusoidal waveform subtracted by the Rectifier 1 waveform. This subtraction happens because Rectifier 2 current signal sensor is placed at the input of the HTR. Thus, for Rectifier 2, it is following the sinusoidal current signal, but the current amplitude drops in the periods in which Rectifier 1 is conducting current [3,12].

An important aspect to achieve control in this type of HTR is to have the control of Rectifier 2 to impose a waveform as shown in Figure 3b. For this, the inductor current signal is obtained through a current sensor at the input of each phase of the HRT, and this can be seen as a control strategy to achieve the desired current waveform. This control strategy is interesting, as it allows samples to be taken of the input currents of the hybrid rectifier and not of the currents in the inductors of Rectifier 2 (which happens in some types of control). This has the advantage of greatly simplifying the practical implementation of the hybrid rectifier. In other control strategies, the sampling of currents in the inductors is obtained in Rectifier 2 and this makes it necessary to create an additional circuit capable of generating the desired reference signal. In this way (as proposed), it has a simpler practical implementation, the adopted control strategy monitors the currents in each of the phases at the input of the hybrid rectifier and compares them with their respective sinusoidal references, thus generating the error signal. With this, Rectifier 2 is forced to impose the necessary current waveform in such a way that, when adding the input currents of Rectifier 1, sinusoidal currents are obtained in the hybrid three-phase rectifier [3,12].

In the proposed HTR, the Rectifier 1 control circuit consists of the UC3854B, current compensator C_{i1}, the peak current limiter LCP_1 (R_{pk1} and R_{pk2}), the power limiter (R_{mo1}), the resistance R_{AC1} and other components, as shown in Figure 9. As for Rectifier 2 (taking module 1 as an example), the control circuit consists of the UC3854B, a current compensator C_{i21}, the current limiter peak LCP_{21} (R_{pk11} and R_{pk21}), the power limiter (R_{mo21}), the resistance R_{AC21} and other components, as represented in Figure 10.

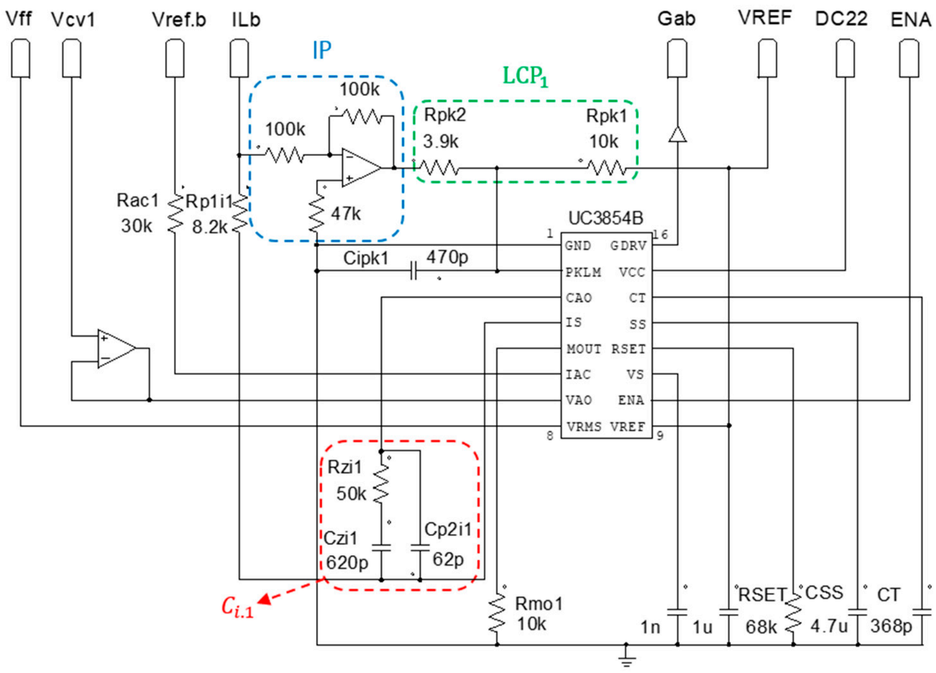

Figure 9. Rectifier 1 control circuit with current limiter peak LCP_1 and polarity inverter IP.

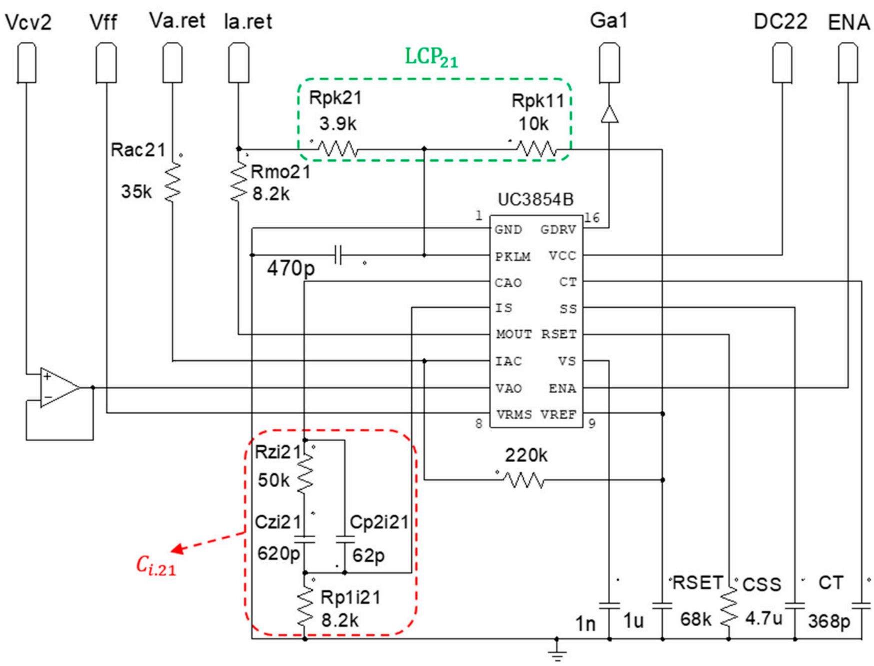

Figure 10. Control circuit in module 1 of Rectifier 2 using current limiter peak LCP_{21}.

The control circuit of Rectifier 1 and Rectifier 2 are connected to the interface circuit through the following terminals:

- G_{ab} (PWM for Rectifier 1 IGBT gate);
- G_{a1} (PWM for Rectifier 2 IGBT gate);
- I_{Lb} (Rectifier 1 Boost inductor current);
- $I_{a,ret}$ (phase A rectified current);

- V_{CV1} (Voltage compensator control voltage for Rectifier 1);
- V_{CV2} (Voltage compensator control voltage for Rectifier 2);
- $V_{ref,b}$ (programmable reference voltage for Rectifier 1);
- $V_{a,ret}$ (programmable reference voltage for Rectifier 2);
- V_{ff} (feed-forward voltage);
- V_{REF} (7.5 V reference voltage);
- DC22V (22 V integrated circuit power supply);
- ENA (5 V power supply for on/off control mode).

In Rectifier 1 control circuit (see Figure 9), the current loop is analyzed from the Boost inductor current signal (terminal I_{Lb}) obtained by means of a current sensor at the positive terminal of the Boost inductor and the signal is thus connected to pin 4 and pin 2 of the UC3854B. It is connected to pin 4 through resistance R_{mo1}, as the pin (inside the UC3854B) has an inverter port to obtain the current signal in negative polarity. To connect to pin 2, an additional circuit is required that reverses the polarity of positive to negative current (IP). The programmable reference voltage signal (terminal $V_{ref,b}$) is connected to pin 6 of the UC3854B through the current limiting resistance R_{AC1}. The output voltage error signal, which is part of the voltage loop, is processed by the voltage compensator and connected to pin 7 (terminal V_{CV1}) through a Buffer, with the function of controlling the output voltage.

In the case of the Rectifier 2 control circuit (see Figure 10), the current loop is analyzed from the rectifier input current signal, the signal being rectified by an RPI (terminal $I_{a,ret}$) that in turn, is connected to pin 5 of the UC3854B through resistance R_{mo21}. The programmable reference voltage signal (terminal $V_{a,ret}$) is connected to pin 6 of the UC3854B, through resistance R_{AC21}, current limiter. The output voltage error signal, which is part of the voltage loop, is also processed by the same voltage compensator that was applied to Rectifier 1, and is connected to pin 7 (terminal V_{CV2}) through a Buffer, with the function to control the output voltage.

3. Simulation Results

Simulations was run in PSIM, for this purpose the power circuits, the interface circuit and the control circuit were applied, as already described in the previous chapters. Table 1 presents the general specifications of the elements used in the simulation.

According to the proposed power distribution between Rectifier 1 and Rectifier 2 55.1% for Rectifier 1 and 44.9% for Rectifier 2, it was necessary to implement the gains of the Rectifier 1 current sensor (G_{SI1}) and Rectifier 2 ($G_{SIa}, G_{SIb}, G_{SIc}$), as shown in Table 1.

Table 1. Specifications system for simulation.

Parameter	Description	Value
$V_{lin,rms}$	rms line voltage	380 V
f_r	Grid frequency	50 Hz
V_o	Rated output voltage	760 V
P_o	Output power	20 kW
R_o	Load	28.88 Ω
C_o	Output Condenser	1100 µF
f_s	Switching frequency	50 kHz
$L_{b1} = L_{b2}$	Rectifier 1 boost inductor	0.8 mH
$L_{11} = L_{12}$	Rectifier 2 Coupled Inductor	2.2 mH
M	Mutual inductance	1.32 mH
G_{SI1}	Rectifier 1 current sensor gain	0.14
$G_{SIa} = G_{SIb} = G_{SIc}$	Rectifier 2 current sensor gain	0.07
G_{Vo}	Output voltage sensor gain	0.00329

3.1. Rectifier Input Parameters

The proposed HTR is fed with a line voltage of 380 V, phased at 120 degrees, which represents a phase voltage of 220 V. Analyzing the input currents in the proposed rectifier, as presented in Figure 11, it is noted that a sinusoidal waveform in each phase, with peak currents of 42.9 A, and this is phased at 120 degrees. This indicates that the currents are being rectified by each rectifier module independently, and correspond to the three-phase system [3,12].

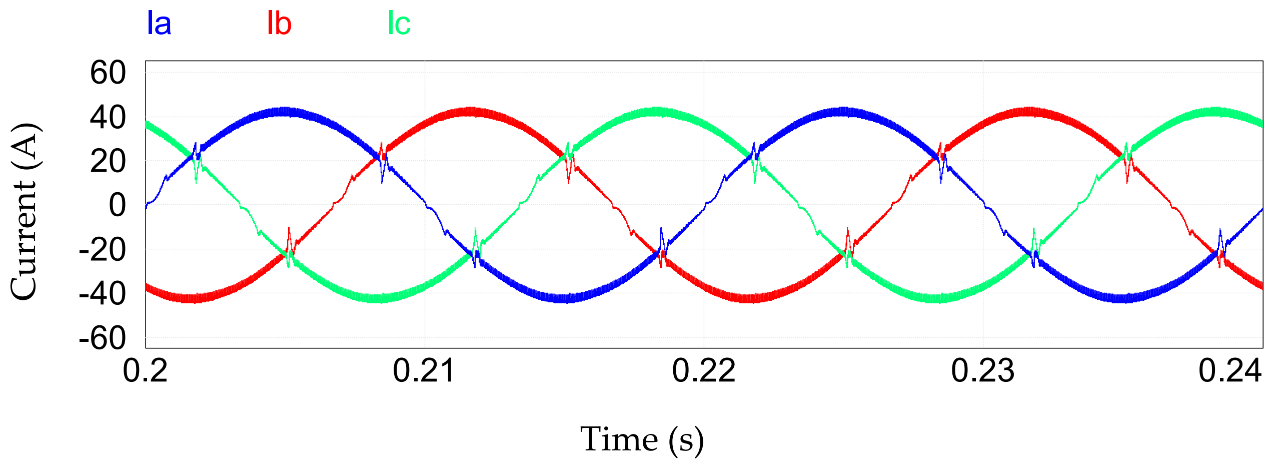

Figure 11. Input current in the three phases of the rectifier.

The PFC with the proposed control system was achieved and this can be observed with the sinusoidal waveform of the current and the phase shift with the respective voltage, in each phase [3,12]. In Figure 12, the voltage and current for each phase of the rectifier are shown (the scale of the current waveform in relation to voltage was separated and increased to allow better visualization). It is noted that in each phase, the current waveform presents the same voltage waveform (it is in phase with the voltage), which allowed obtaining a PF of 99.92% and a THD the current of 3.96% also, indicated in Table 2. These values allow us to conclude that the proposed rectifier operates below the limit values recommended by international standards (THD = 5%), namely IEEE 519 and IEC61000-3-2 [26,27], which ensures the quality of the power grid using the proposed rectifier.

Table 2. Power distribution, PF and THD, in phase A, phase B and phase C.

Phase	V_{ef} (V)	I_{ef} (A)	S (kVA)	P (kW)	PF (%)	THD (%)
Phase A	220	30.33	6.653	6.648	99.92	3.96
Phase B	220	30.32	6.649	6.643	99.92	3.96
Phase C	220	30.33	6.654	6.649	99.92	3.96

In Table 2, the effective currents I_{ef} per phase of the rectifier are indicated, as well as the apparent power and active power. Thus, the total apparent power S is 20 kVA. The power factor is 99.92%, and the total active power P is 19.94 kW.

Since the HTR is composed of two rectifiers (Rectifier 1 and Rectifier 2), it is noted that the peak current obtained at the input of the HTR has a value of the order of 43 A per phase. This value is made up of the Rectifier 1 peak current of 21.5 A and the Rectifier 2 peak current of 21.5 A. This allows us to conclude that the peak current distribution between the rectifiers is 50% [3,4,12], presented in Figure 13. The current waveforms in phase A, of the hybrid rectifier, seen in Figure 13, show the expected waveforms, that is, Rectifier 1 generated a rectangular waveform (Ia1) and Rectifier 2 generated a waveform (Ia2) such that, when adding the two waveforms, a sinusoidal wave form was obtained in the HTR phase (Ia).

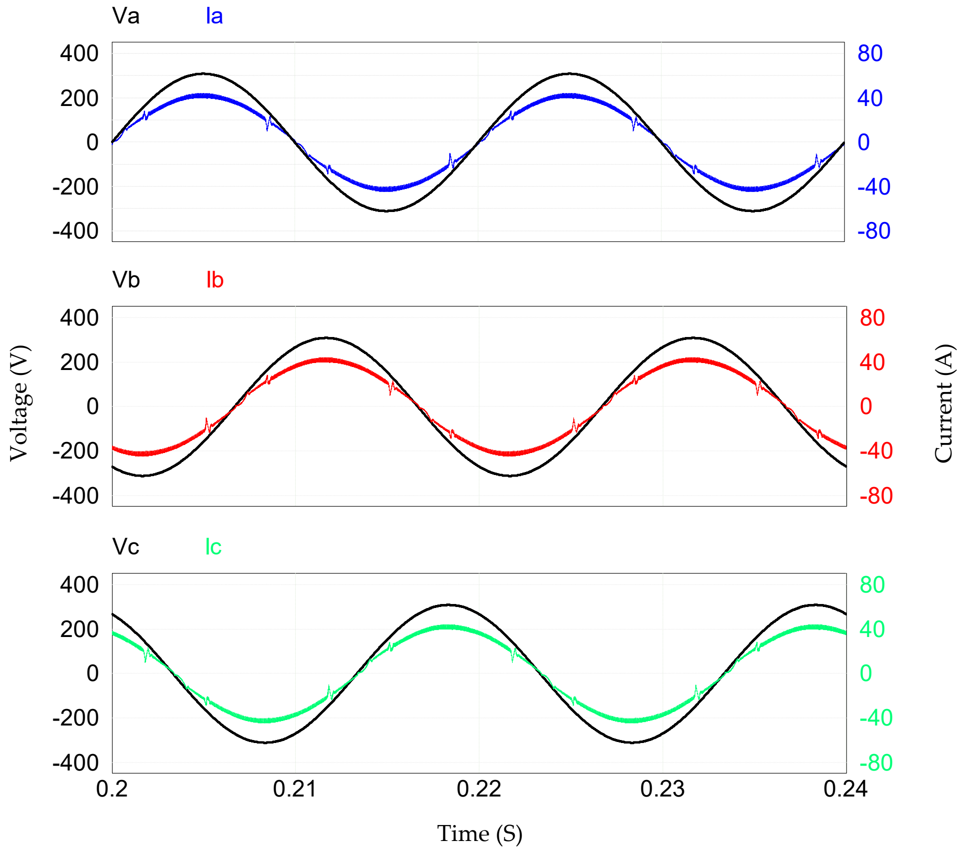

Figure 12. Voltage and current in phase A (Va, Ia), phase B (Vb, Ib), and phase C (Vc, Ic).

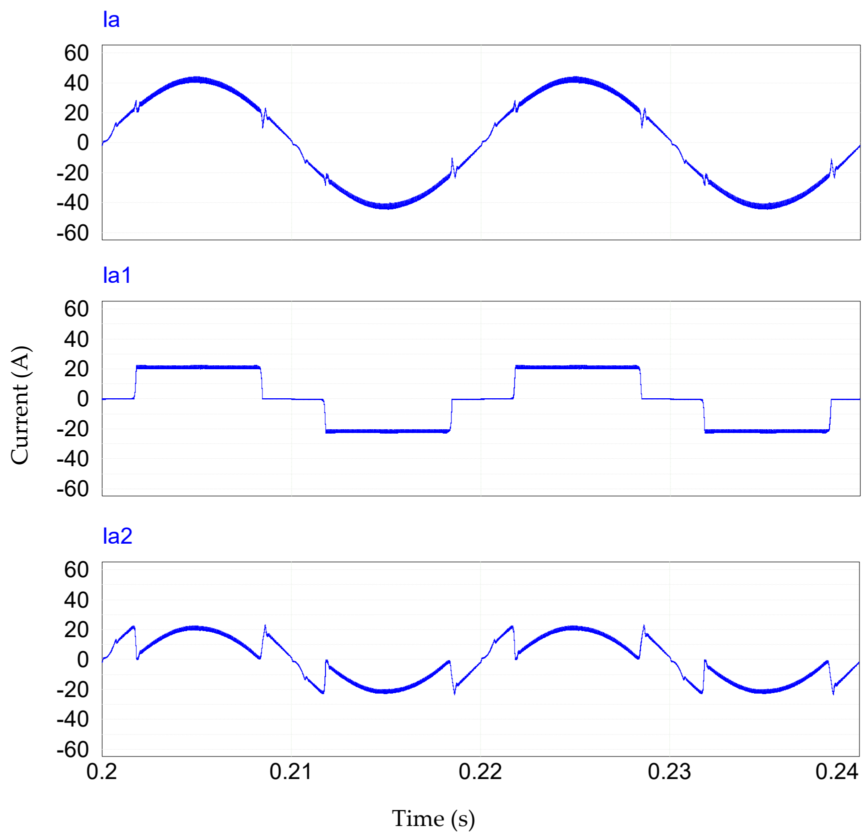

Figure 13. Current waveform in phase A, of the hybrid rectifier (Ia), of Rectifier 1 (Ia1) and of Rectifier 2 (Ia2).

Through the 50 kHz switching frequency of the Boost converter in each rectifier module, the input current waveform in the proposed rectifier presents a current ripple. This current ripple is shown in Figure 14 (referring to phase A), representing a ripple of approximately 3 A. A deformation in the shape of the current ripple is noted, which is due to the fact that it is a wave obtained by the sum of two current waves (Rectifier 1 and Rectifier 2), which are not synchronized, thus presenting a small phase difference between them, which is shown in Figure 15. It is important to highlight that this does not affect the operation of the HTR.

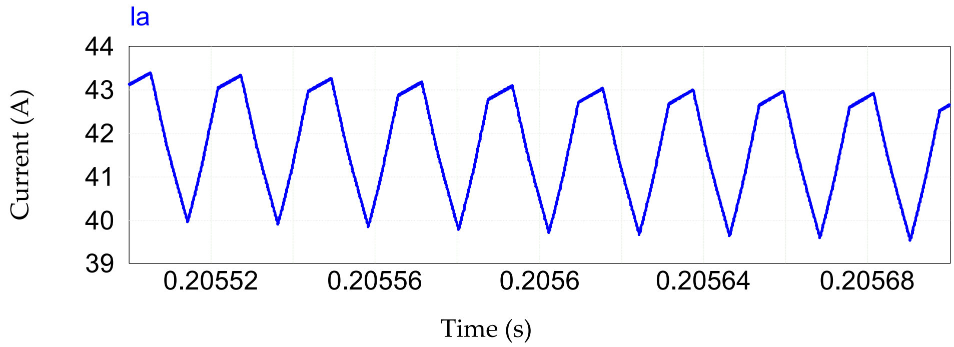

Figure 14. Input current ripple in phase A of the hybrid rectifier.

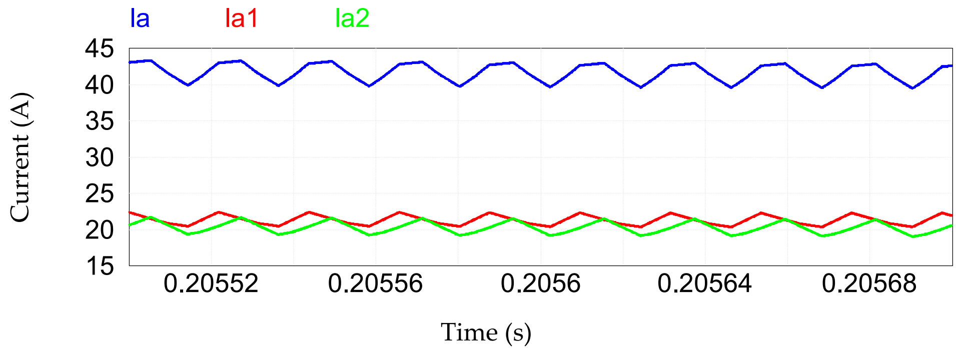

Figure 15. Input current ripple in phase A of the hybrid rectifier (Ia); of Rectifier 1 (Ia1) and Rectifier 2 (Ia2).

To observe the frequencies that make up the waveforms as the three currents obtained (I_a, I_b, I_c), the Fast Fourier Transform (FFT) was applied, shown in Figure 16. It is observed that the currents are basically composed only of the fundamental frequency 50 Hz. This analysis presents the fundamental frequency and some harmonics with very low values that can be disregarded.

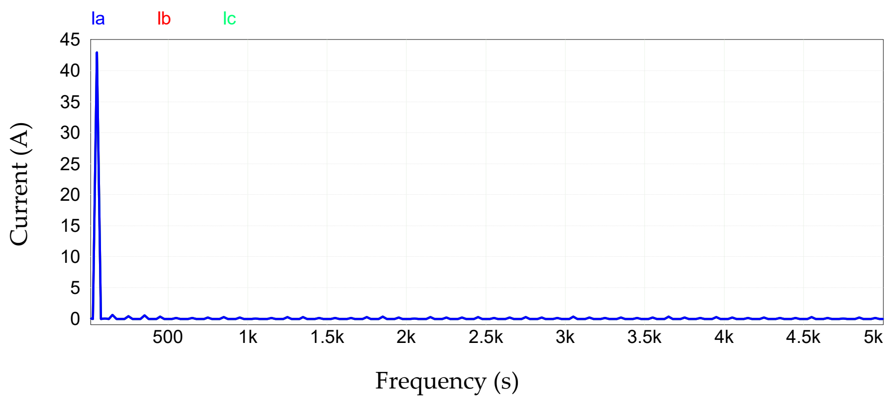

Figure 16. Fast Fourier analysis of currents, I_a, I_b and I_c.

3.2. Rectifier Output Parameters

Observing the behavior of the output voltage and current of the proposed three-phase hybrid rectifier, in Figure 17, the dynamic range for both quantities is similar. It is observed that at the beginning of the transient period, the output voltage rises to a value of 875 V, and adjusts until it reaches a stable value of 760 V in 0.1 s. The output current also has a similar behavior, reaching a peak value of 30 A and then (after 0.1 s) stabilizing to a value of 26.3 A.

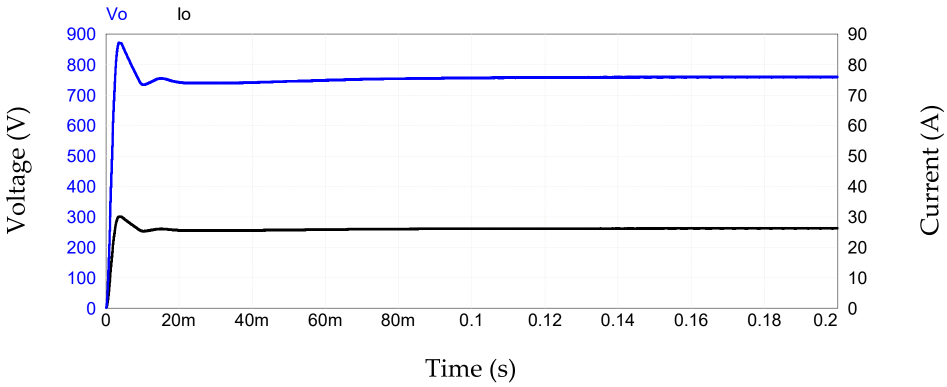

Figure 17. Transient period of the hybrid rectifier output voltage and current driving.

In the case of output voltage ripple, it presents a very low value that is practically negligible, as shown in Figure 18, this is because the output capacitor was sized according to the hold-up time criterion [3,12].

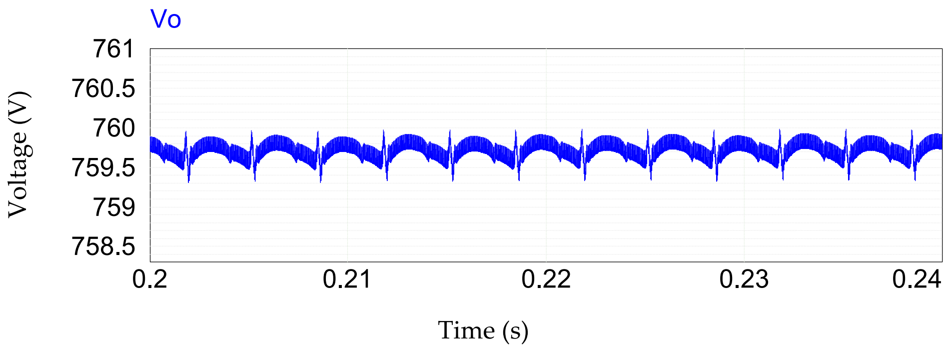

Figure 18. Transient period of the hybrid rectifier output voltage and current.

3.3. Rectifier Performance

In order to verify the dynamic behavior of the control loops, a load variation test was carried out from the nominal value (100%) to 50%. Initially, the system works with 100% load, in a period of 0.55 s the load drops to 50%, and later (after 0.1 s) in 0.65 s the load is increased to 100% again. This test made it possible to observe the following behaviors (both at the rectifier input and at the rectifier output).

For the input of the hybrid three-phase rectifier, a dynamic behavior was observed, as shown in Figure 19. It is noted that in this analysis, when the 0.55 s period begins, the current decreases in amplitude and the control system acts causing that in approximately 0.57 s the current becomes stable, then a period of 0.65 s arrives in which 100% is activated, it is observed that the current increases smoothly until it reaches the nominal current value in approximately 0.675 s. It was also found that the load variation affected Rectifier 1 and Rectifier 2 in equal proportion.

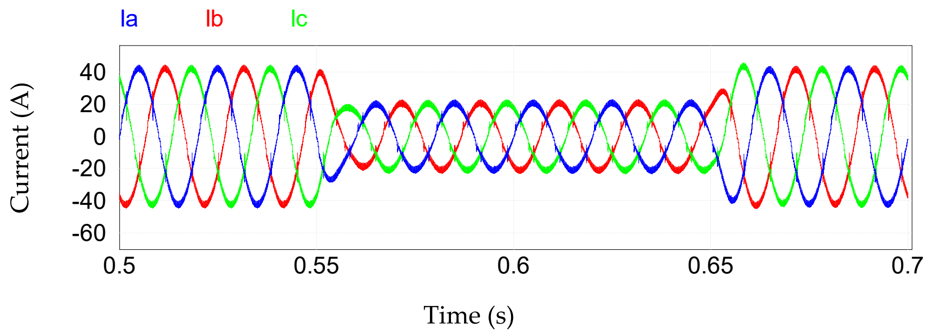

Figure 19. Input currents variation which the load is champed to 50%.

For the output of the hybrid three-phase rectifier, the current is shown in Figure 20 and the voltage in Figure 21. Initially, there is a nominal current of 26.31 A, and voltage of 760 V. At the instant (0.55 s) in which the load goes from 100% to 50%, the current drops in value and stabilizes in 0.6 s to a value of 13.15 A, at this same instant of 0.5 s there is a sudden increase in the output voltage, reaching a maximum value of 790 V in 0.565 s, which stabilizes to 760 V in 0.625 s. The charge then goes to 100% in 0.65 s, in this case the current shows a small ripple and stabilizes at 26.31 A in 0.68 s, while the voltage drops sharply, reaching a value of 728 V (thus, it showed the same voltage behavior during the 50% load reduction period). Note that the output voltage takes longer time to stabilize, which is due to the high value of the output capacitor C_o.

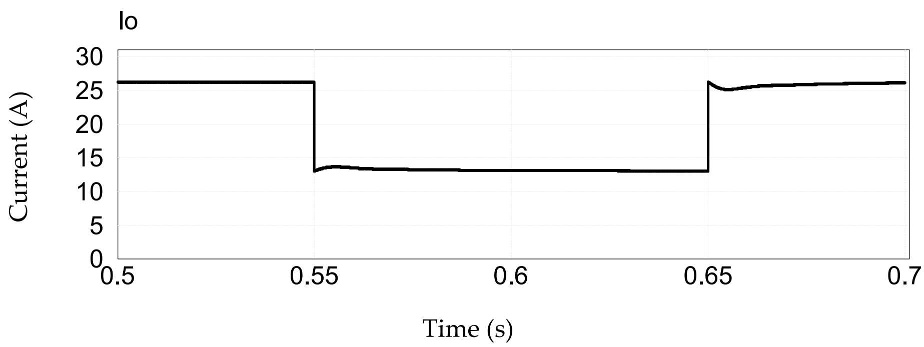

Figure 20. Hybrid rectifier output current with 50% load variation.

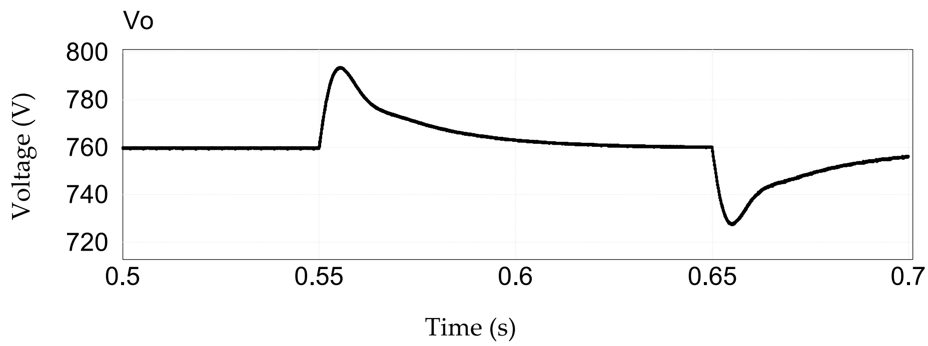

Figure 21. Hybrid rectifier output voltage with 50% load variation.

3.4. Power Distribution

For a detailed analysis of the power distribution in the hybrid rectifier (HR), Table 3 shows the power distribution in each phase of Rectifier 1 and Rectifier 2. Note that in total, the power distribution between Rectifier 1 and Rectifier 2, was very close to the target of 55.1% in Rectifier 1 and 44.9% in Rectifier 2 [3,12]. Thus, it is proving that the proposed hybrid rectifier simulation works with a correct distribution.

Table 3. Simulation values of power distribution in Rectifier 1 (R1) and Rectifier 2 (R2).

Phase	P(kW)-R1	P(kW)-R2	P(kW)-HR	P(%)-R1	P(%)-R2
Phase A	3.639	3.009	6.648	54.74	45.26
Phase B	3.640	3.008	6.648	54.75	45.25
Phase C	3.640	3.009	6.649	54.75	45.25
Total	10.92	9.03	19.95	54.75	45.28

In Section 2.2 of the interface circuit, the circuit implemented to limit the current level between Rectifier 1 and Rectifier 2, shown in Figure 7, was described. Note that varying the resistance R_{GCV} varies the amplifier gain and consequently varies the level of chain. In this case, to vary the current level of Rectifier 1, the resistance R_{GCV1} of the circuit itself must be varied. To vary the current level of Rectifier 2, the resistance R_{GCV2} of the circuit itself must be varied. Note that by varying the current level of one rectifier, consequently the other rectifier also varies, in order to compensate and maintain total power [12].

In the case of correct power distribution, the value of $R_{GCV1} = 5$ kΩ, indicated (highlighted in color) in Table 4.

To prove the functioning of this system, two tests were carried out, changing the value of R_{GCV1}. The first test was with $R_{GCV1} = 3$ kΩ, and the second test was with $R_{GCV1} = 8$ kΩ.

For $R_{GCV1} = 3$ kΩ, it is noted that the current in Rectifier 1 decreased in level and consequently Rectifier 2 increased in level [4,12], as shown in Figure 22. It is also noted that the sinusoidal waveform has higher quality and consequently improved PF and THDi, indicated in Table 4. In the second test, $R_{GCV1} = 8$ kΩ, it is noted that there was an increase in the current of Rectifier 1, and consequently lowered the current of Rectifier 2 [4,12], it is shown in Figure 23. It is also noted that the waveform of HTR input current was deformed and consequently worsened the PF and THDi [4,12], indicated in Table 4.

Table 4. Power distribution varying the resistance R_{GCV1}.

R_{GCV1} (kΩ)	P (kW)-R1	P (kW)-R2	P (kW)-HR	P (%)-R1	PF (%)	THDi (%)
3	5.96	13.98	19.94	29.89	99.93	3.45
5	10.92	9.02	19.94	54.75	99.92	3.96
8	15.21	4.73	19.94	76.28	99.68	7.97

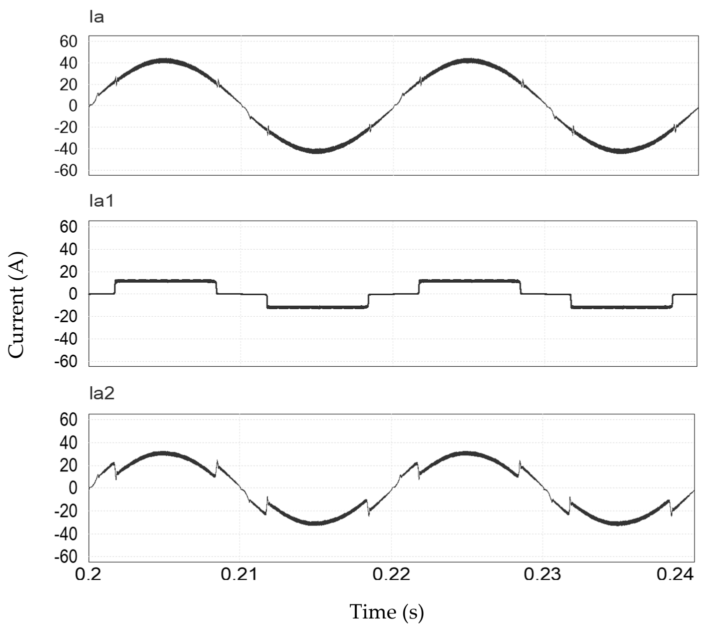

Figure 22. Input current in phase A of the hybrid rectifier, for $R_{GCV1} = 3$ kΩ.

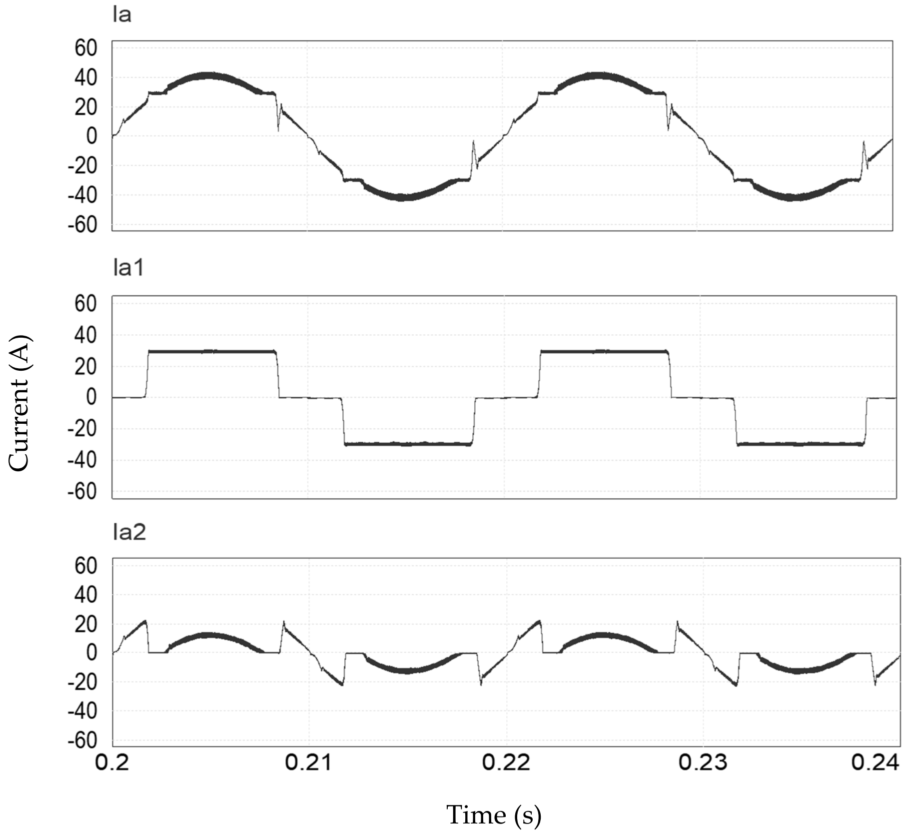

Figure 23. Input current in phase A of the hybrid rectifier, for $R_{GCV1} = 8$ kΩ.

Note that in this test only the R_{GCV1} resistance was varied. It was also observed that by varying the resistance R_{GCV2} (Rectifier 2) in the same proportion as the resistance R_{GCV1}, the behavior of the currents is similar.

3.5. Comparison

Table 5 illustrates a comparison of the values obtained in the proposed HTR with the HTR found in the literature. Thus, the proposed HTR is compared with an HTR with a Boost converter (HTR Boost), an HTR with a SEPIC converter (HTR SEPIC), and two types of HTR with a Vienna converter (HTR Vienna).

Table 5. Comparison of the proposed HTR with the HTR found in the literature.

HTR	Reference	P (kW)-HR	P (%)-R1	P (%)-R2	PF (%)	THDi (%)
HTR Proposed		20	54.75	45.28	99.92	3.96
HTR Boost	[3]	20	55.2	44.8	99.89	4.54
HTR SEPIC	[28]	5	60	40	98	3.75
HTR Vienna	[5]	21	55.2	44.8	98.89	7.9
HTR Vienna	[25]	20	55.2	44.8		3.22

In terms of power distribution, it is observed that the proposed rectifier presents a distribution very close to the intended one of 55.1% in Rectifier 1 and 44.9% in Rectifier 2, which was also achieved in HTR Boost [3], and to the two HTR Vienna [5,25]. The HTR SEPIC, on the other hand, presents a different distribution than the other rectifiers, but in a somewhat interesting way (because in an HTR it is desired that Rectifier 1 processes the largest portion of power), because although Rectifier 1 processes approximately 60% of total power, has high PF and low THDi.

Note that in terms of PF, the proposed HTR presents a higher value, but not very different from the other HTR, thus proving correct operation of the applied control, as well as the voltage and current sensors and the respective precision rectifiers. At THDi, the proposed HTR, HTR Boost [3], HTR SEPIC [28], and HTR Vienna operate below the limit values recommended by international standards (THD = 5%), namely IEEE 519 and IEC61000-3-2/IEC61000-3-4, thus guaranteeing the quality of the electrical network. The other HTR Vienna [5], operates above the limit value recommended by international standards (THD = 5%). It is believed that the difference has to do with the fact that the values presented in HTR Vienna [5] were obtained through a prototype, and the others were obtained through simulation. Thus, this comparison somewhat validates the results obtained in the proposed HTR.

4. Conclusions

Analyzing the results obtained, it is considered that in an RTH with Boost converter without isolation transformer this can be achieved if the boost converter inductor of Rectifier 2 is replaced by a coupled inductor. Both the development of the coupled inductor and the methodology for connecting the power circuit with the control circuit through the interface circuit prove to be viable, as it allows the mitigation of current interaction and the decoupling between the two circuits (power and control). In this sense, the correct functioning of the voltage and current precision rectifier circuit was also verified, as well as the input voltage sensor circuit and the feed-forward voltage generator circuit.

The control circuit was modeled and developed using UC3854B and proved to be viable, since output voltage stability (760 V) was achieved, a high PF of 99.92% and a low THD of 3.96% were also obtained, and even capable of meeting international standards. A correct power distribution between the rectifiers was also achieved, with 55.1% in Rectifier 1 and 44.9% in Rectifier 2. Also, it was proven that through the current level regulator circuit, it is possible to make an adjustment in the power distribution between the two rectifiers.

Author Contributions: Conceptualization, J.T.G. and S.V.; methodology, J.T.G.; software, J.T.G.; validation, S.V. and F.B.; formal analysis, F.B. and E.L.; investigation, J.T.G. and S.V.; resources, J.T.G. and E.L.; writing—original draft preparation, J.T.G. and S.V.; writing—review and editing, J.T.G. and F.B.; visualization, J.T.G. and E.L.; supervision, S.V. and F.B.; project administration, J.T.G. and S.V.; funding acquisition, J.T.G. and E.L. All authors have read and agreed to the published version of the manuscript.

Funding: This research received no external funding.

Data Availability Statement: Data is contained within the article.

Conflicts of Interest: The authors declare no conflict of interest.

References

1. Kolar, J.W.; Ertl, H. Status of the Techniques of Three-phase Rectifier Systems with Low Effects on the Mains. In Proceedings of the 21st International Telecommunications Energy Conference INTELEC '99 (Cat No99CH37007), Copenhagen, Denmark, 9 June 1999; pp. 11–14.
2. Alves, R.L. Concepção e Análise de Retificadores Híbridos Trifásicos Unidirecionais. Doctoral's Thesis, Universidade Federal de Santa Catarina, Florianópolis, Brazil, 2008.
3. Gonçalves, J.T.; Valtchev, S.; Melicio, R.; Al-Saadi, M. Three-Phase Unidirectional Transformerless Hybrid Rectifier with Boost Converter. In Proceedings of the 2019 IEEE 1st Global Power, Energy and Communication Conference, GPECOM, Nevsehir, Turkey, 12–15 June 2019; pp. 158–163.
4. Gonçalves, J.T.; Valtchev, S.; Melicio, R.; Gonçalves, A.; Blaabjerg, F. Hybrid Three-Phase Rectifiers with Active Power Factor Correction: A Systematic Review. *Electronics* **2021**, *10*, 1520. [CrossRef]
5. Alves, R.L.; Barbi, I. Analysis and Implementation of a Hybrid High-Power-Factor Three-Phase Unidirectional Rectifier. *IEEE Trans. Power Electron.* **2009**, *24*, 632–640. [CrossRef]
6. De Freitas, L.C.G.; Coelho, E.A.A.; Finazzi, A.P.; Simoes, M.G.; Canesin, C.A.; de Freitas, L.C. Programmable PFC based hybrid multipulse power rectifier for utility interface of power electronic converters. In Proceedings of the 2005 IEEE 36th Power Electronics Specialists Conference, Dresden, Germany, 16 June 2005; IEEE: Piscataway, NJ, USA, 2005; pp. 2237–2243.
7. De Freitas, L.C.G.; Vincenzi, F.; Freitas, M.A.A.; Fernandes, E.R.; Mendonça, R.G.; de Freitas, L.C. Programmable PFC Based Hybrid Multipulse Power Rectifier with Sinusoidal Input Line Current Imposed by Digital Controller. In Proceedings of the

IEEE APEC 07—Twenty-Second Annual IEEE Applied Power Electronics Conference and Exposition, Anaheim, CA, USA, 25 February–1 March 2007; pp. 1356–1361.
8. De Freitas, L.C.G.; Coelho, E.A.A.; Parreira, É.F.; Oliveira, M.A.G.; de Freitas, L.C. Multipulse Power Rectifier without Using Multiphase Transformers. In Proceedings of the 31st Annual Conference of IEEE Industrial Electronics Society, 2005 IECON 2005, Raleigh, NC, USA, 6–10 November 2005; IEEE: Piscataway, NJ, USA, 2005; pp. 519–524.
9. Bai, L.; Wang, D.; Zhou, Y. Study on the Current Control Strategy of Hybrid Rectifier based on the PR Controller. In Proceedings of the International Conference on Electrical Machines and Systems (ICEMS), Busan, Republic of Korea, 26–29 October 2013; pp. 1693–1696.
10. De Freitas, L.C.G.; Simoes, M.G.; Canesin, C.A.; de Freitas, L.C. Programmable PFC Based Hybrid Multipulse Power Rectifier for Ultra Clean Power Application. *IEEE Trans. Power Electron.* **2006**, *21*, 959–966. [CrossRef]
11. De Freitas, L.C.G.; Simões, M.G.; Canesin, C.A.; de Freitas, L.C. Performance Evaluation of a Novel Hybrid Multipulse Rectifier for Utility Interface of Power Electronic Converters. *IEEE Trans. Ind. Electron.* **2007**, *54*, 3030–3041. [CrossRef]
12. Gonçalves, J.T. Desenvolvimento de um Retificador Trifásico Híbrido Unidirecional com Conversor Boost. Doctoral's Thesis, NOVA School of Science and Technology, Caparica, Portugal, 2022.
13. Mayergoyz, I.D.; Lawson, W. *Basic Electric Circuit Theory: A One-Semester Text*; Gulf Professional Publishing: Houston, TX, USA, 1997; pp. 382–400.
14. Zhang, Z. *Coupled-Inductor Magnetics in Power Electronics*; California Institute of Technology: Pasadena, CA, USA, 1987.
15. Sundararajan, D. *Introductory Circuit Theory*; Springer International Publishing: Berlin/Heidelberg, Germany, 2020; Volume 258, pp. 177–201.
16. Brusamarello, V.J.; Blauth, Y.B. An analysis of k ii coupling coefficients. *Int. J. Electr. Eng. Educ.* **2012**, *49*, 16–25. [CrossRef]
17. Font, C.H.I. Retificadores Trifásicos HIíbridos Bidirecioanais com Fator de Potência Unitário. Doctoral's Thesis, Florianópolis, Brazil, 2009. Available online: http://repositorio.ufsc.br/xmlui/handle/123456789/92783 (accessed on 7 May 2024).
18. Rossetto, L.; Spiazzi, G.; Tenti, P. Control techniques for power factor correction converters. In Proceedings of the Power Electronic, Motion Control (PEMC), Warsaw, Poland, 20–22 September 1994; pp. 1310–1318. Available online: https://citeseerx.ist.psu.edu/document?repid=rep1&type=pdf&doi=cfed95f1348fe56119c8d1376023f238a2e691d8 (accessed on 7 May 2024).
19. Silva, C.d.S. *Power Factor Correction with the UC3854*; Application Note; Unitrode Integr Circuits Corp.: Merrimack, NH, USA, 1995.
20. Redl, R.; Balogh, L. RMS, DC, Peak, and Harmonic Current in High-Frequency Power-Factor Correctors with Capacitive Energy Storage. In Proceedings of the APEC '92 Seventh Annual Applied Power Electronics Conference and Exposition, Boston, MA, USA, 23–27 February 1992; pp. 533–540.
21. Balogh, L.; Redl, R. Power-Factor Correction with Interleaved Boost Converters in Continuous-Inductor-Current Mode. In Proceedings of the Eighth Annual Applied Power Electronics Conference and Exposition, San Diego, CA, USA, 7–11 March 1993; pp. 168–174.
22. Andreycak, B. Optimizing Performance in UC3854 Power Factor Correction Applications. In *Unitrode Design Note DN-39E Texas Instruments*; Texas Instruments Incorporated: Dallas, TX, USA, 1999; Available online: https://www.ti.com/lit/an/slua172/slua172.pdf?ts=1700675470810 (accessed on 7 May 2024).
23. Alves, R.L.; Barbi, I. A New Hybrid High Power Factor Three-Phase Unidirectional Rectifier. In Proceedings of the 2006 IEEE International Symposium on Industrial Electronics, Scottsdale, AZ, USA, 8–11 May 2006; IEEE: Piscataway, NJ, USA, 2006.
24. Font, C.H.I.; Barbi, I. A New High Power Factor Bidirectional Hybrid Three-Phase Rectifier. In Proceedings of the Twenty-First Annual IEEE Applied Power Electronics Conference and Exposition, APEC '06, Dallas, TX, USA, 19–23 March 2006; IEEE: Piscataway, NJ, USA, 2006; pp. 1300–1306.
25. Alves, R.L.; Font, C.H.I.; Barbi, I. Novel Unidirectional Hybrid Three-Phase Rectifier System Employing Boost Topology. In Proceedings of the IEEE 36th Power Electronics Specialists Conference, Recife, Brazil, 12–16 June 2005; IEEE: Piscataway, NJ, USA, 2005; pp. 487–493.
26. Duffey, C.K.; Stratford, R.P. Update of harmonic standard IEEE519: IEEE recommended practices and requirements for harmonic control in electric power systems. *IEEE Trans. Ind. Appl.* **1989**, *25*, 1025–1034. [CrossRef]
27. *IEC 61000-3-2*; Electromagnetic Compatibility (emc)-Part 3: Limits-Section 2: Limits for Harmonic Current Emissions (Equipment Input Current < 16a Per Phase). International Electrotechnical Commision (IEC): Geneva, Switzerland, 2009.
28. Costa, A.V.; Rodrigues, D.B.; de Lima, G.B.; de Freitas, L.C.; Coelho, E.A.A.; Farias, V.J.; Freitas, L.C.G. New hybrid high-power rectifier with reduced THDI and voltage-sag ride-through capability using BOOST converter. *IEEE Trans. Ind. Appl.* **2013**, *49*, 2421–2436. [CrossRef]